

Supporting Information

pH-dependence in facet-selective photo-deposition of metals and metal oxides on semiconductor particles

YuXi Guo^{1,3†}, Igor Siretanu^{2†}, YiHe Zhang^{1*}, Bastian Mei³, Xiaowei Li¹,
Frieder Mugele², Hongwei Huang^{1*}, Guido Mul^{3*}*

¹Beijing Key Laboratory of Materials Utilization of Nonmetallic Minerals and Solid Wastes, National Laboratory of Mineral Materials, School of Materials Science and Technology, China University of Geosciences, Beijing 100083, China

²Physics of Complex Fluids Group and MESA+ Institute, Faculty of Science and Technology, University of Twente, PO Box 217, 7500 AE Enschede, The Netherlands

³Photocatalytic Synthesis Group, MESA+ Institute for Nanotechnology, University of Twente, P.O. Box 217, 7500 AE Enschede, The Netherlands

[†]These authors contributed equally to this work.

* Corresponding authors: zyh@cugb.edu.cn, i.siretanu@utwente.nl,
hhw@cugb.edu.cn, g.mul@utwente.nl

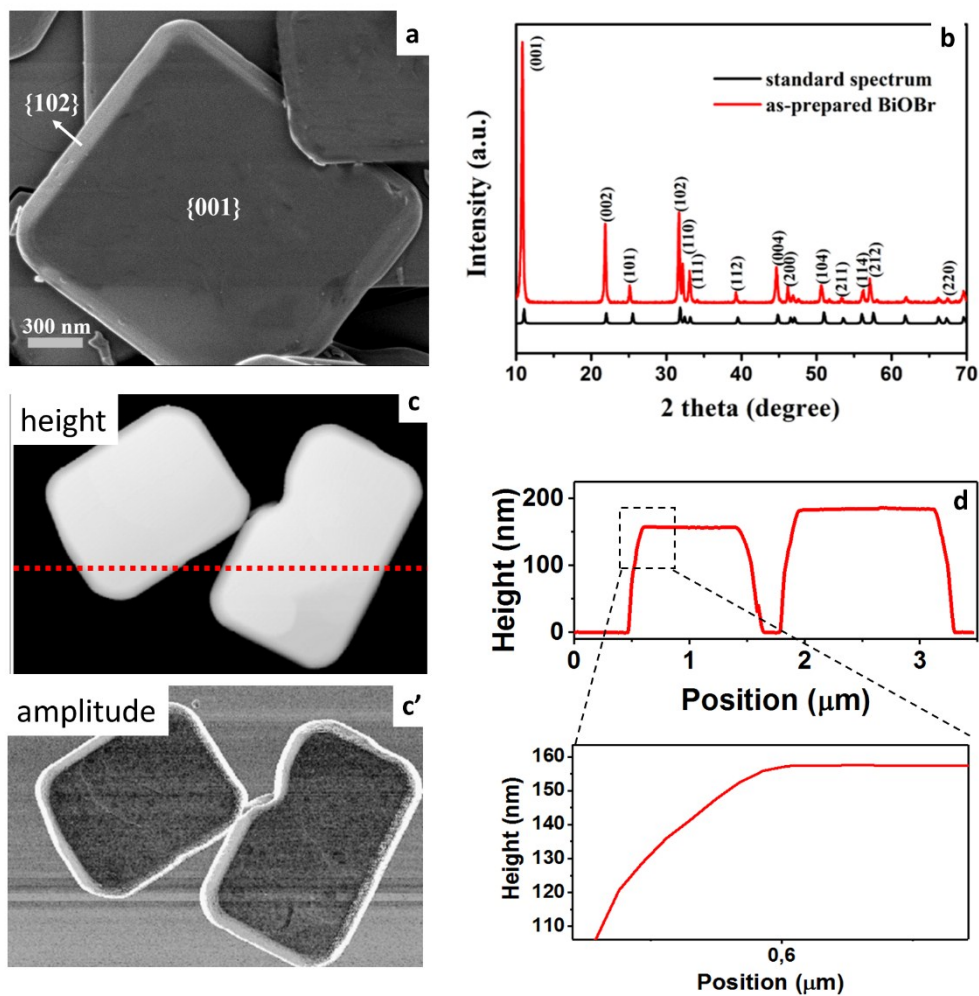


Figure S1. (a) SEM images of BiOBr crystals (without deposited particles). (b) XRD patterns of the plate-like BiOBr. (c) Non-contact AFM topography and amplitude (c') images of BiOBr nanoparticles adsorbed on a Pt substrate in 10 mM NaCl solution (d) corresponding scan line showing the height distribution of the particles.

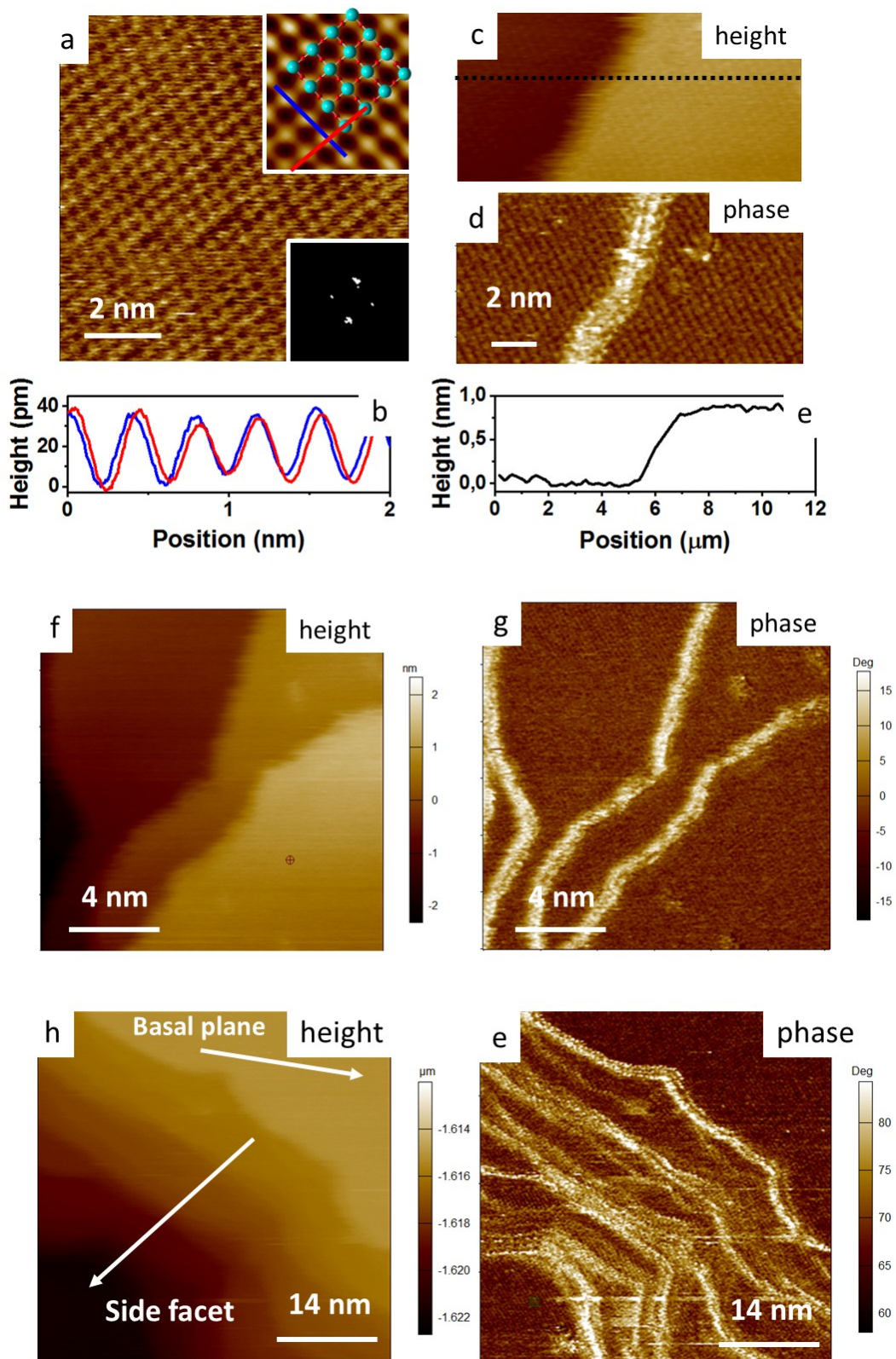


Figure S2 a) AFM topographic image at the atomic scale of a BiOBr basal plane in contact with ultrapure de-ionised water. Insets: zoomed and Fourier-filtered view with superimposed the

crystallographic lattice (top right); 2D fast Fourier transform of the image (down right). b) Height profiles in *a* (red) and *b* (blue) directions display periodicities of 0.39 nm and 0.387 nm consistent with the crystallographic data. (c) Atomic resolution topography image, (d) phase images revealing a step-edge on the BiOBr particle basal plane, with the height difference shown in (e). (f) Atomic resolution topography and phase images (g) of basal planes of BiOBr displaying a region with a well-ordered square structure and regions with disordered non-periodic structures and monatomic and larger steps. (h) Atomic resolution topography and phase images (e) close to the edge of the particle or side plane, displaying a non-periodic structure and steps. The strong contrast in the phase images between smooth topography (terraces) and areas which are more irregular, containing various structural defects, indicates that the tip-sample interaction becomes locally 'less sticky' than elsewhere on the ideal surface, consistent with a different local surface chemistry, such as a broken bond. The observed features in our images thus prove that the surface chemistry (charge in region with steps is more negative comparing to smooth terraces) and/or the hydration structure are modified locally on a sub-unit cell scale.

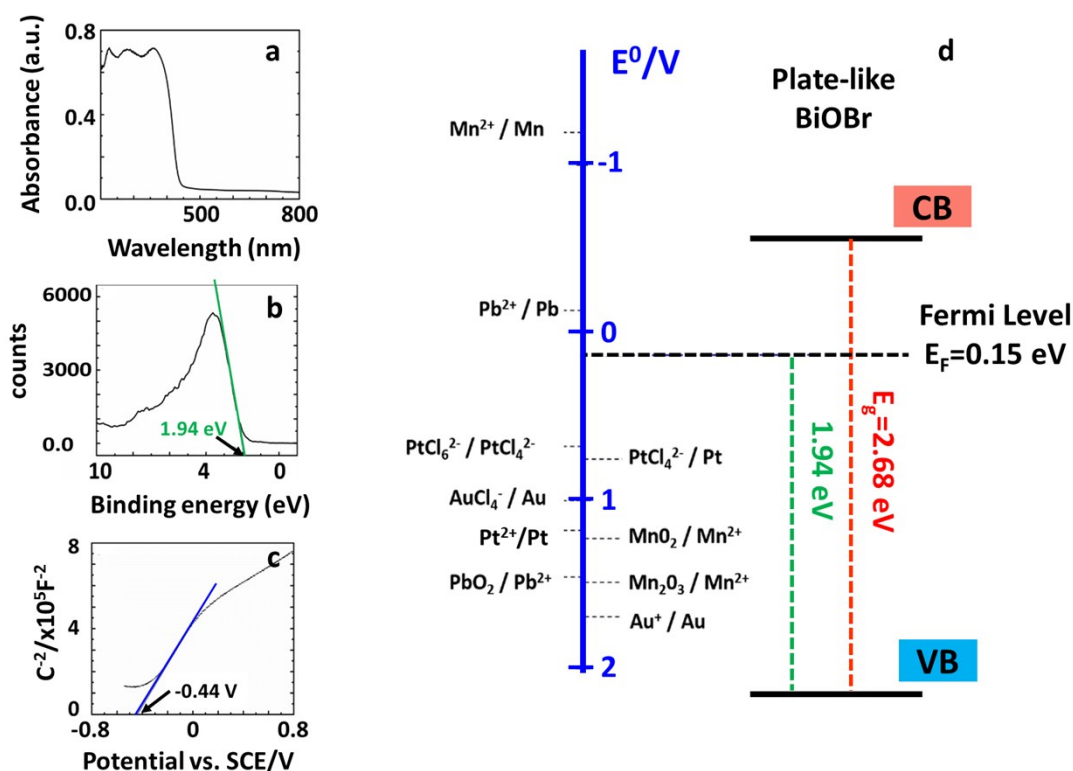


Figure S3. a) UV-vis DRS spectra, b) valence band XPS spectra, c) Mott–Schottky plot, and (d) proposed band structures of BiOBr nanoparticles. Redox potentials of Pt, Au, Pb and Mn-ions or shown for reference.

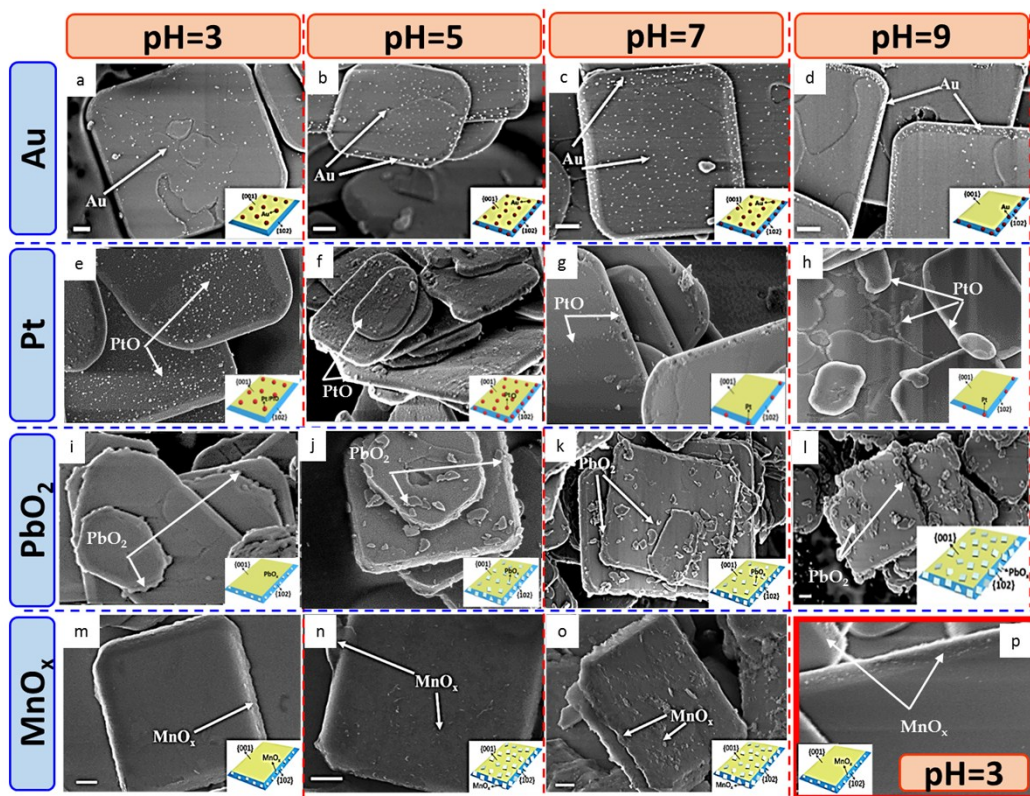


Figure S4. SEM images of BiOBr with a single metal/oxide deposited at different pH values: Au/BiOBr at (a) pH 3; (b) pH 5; (c) pH 7; (d) pH 9; Pt/BiOBr at (e) pH 3; (f) pH 5; (g) pH 7; (h) pH 9; PbO₂/BiOBr at (i) pH 3; (j) pH 5; (k) pH 7, (h) pH 9. MnO_x/BiOBr at (m) pH 3; (n) pH 5; (o) pH 7. (p) SEM image of MnO_x/BiOBr at pH 3, where H₂SO₄ was used to adjust the pH of the MnSO₄ solutions.

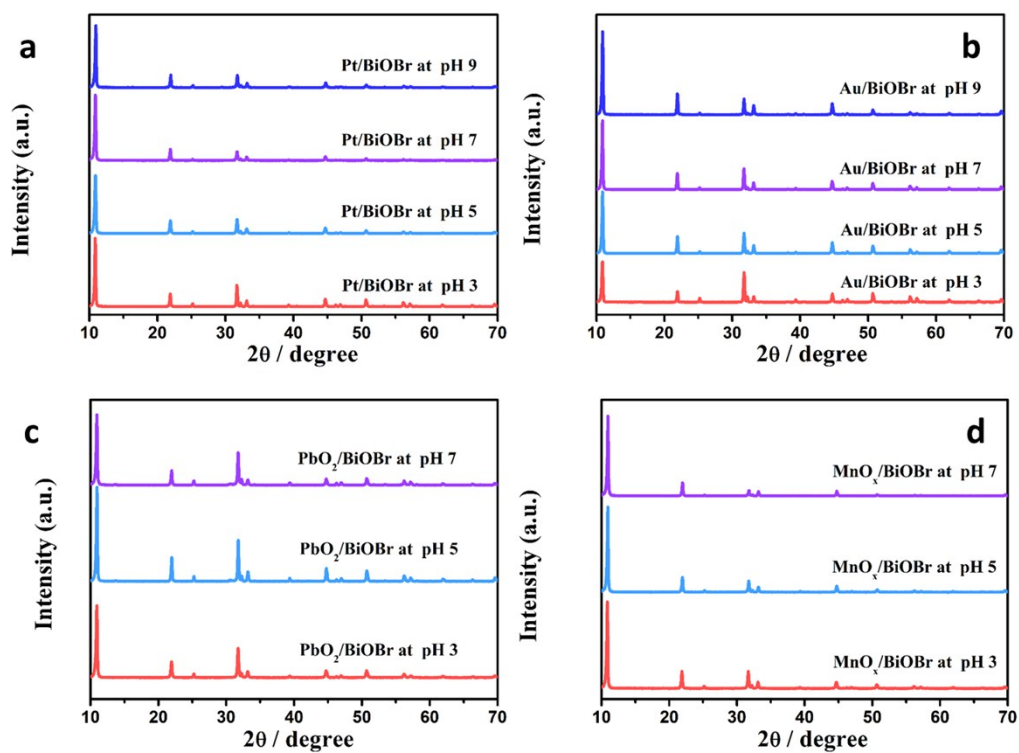


Figure S5. XRD patterns of typical samples after photodeposition at different pH values.

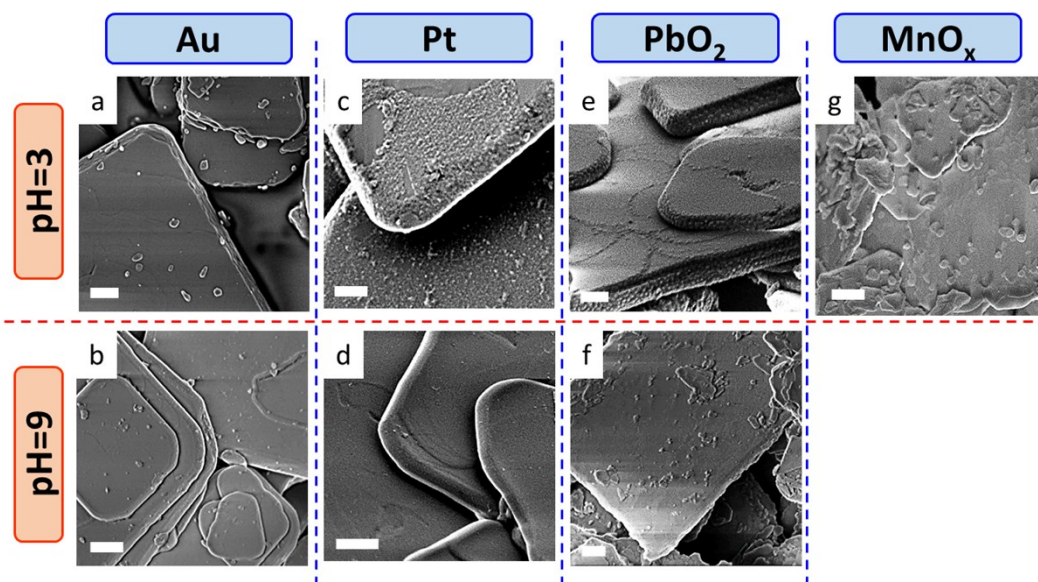


Figure S6. SEM images of typical samples prepared by impregnation at pH 3 and pH 9. (a and b) Au/BiOBr, (c and d) Pt/BiOBr, (e and f) $\text{PbO}_2/\text{BiOBr}$, (g) $\text{MnO}_x/\text{BiOBr}$. Scale bar 200 nm.

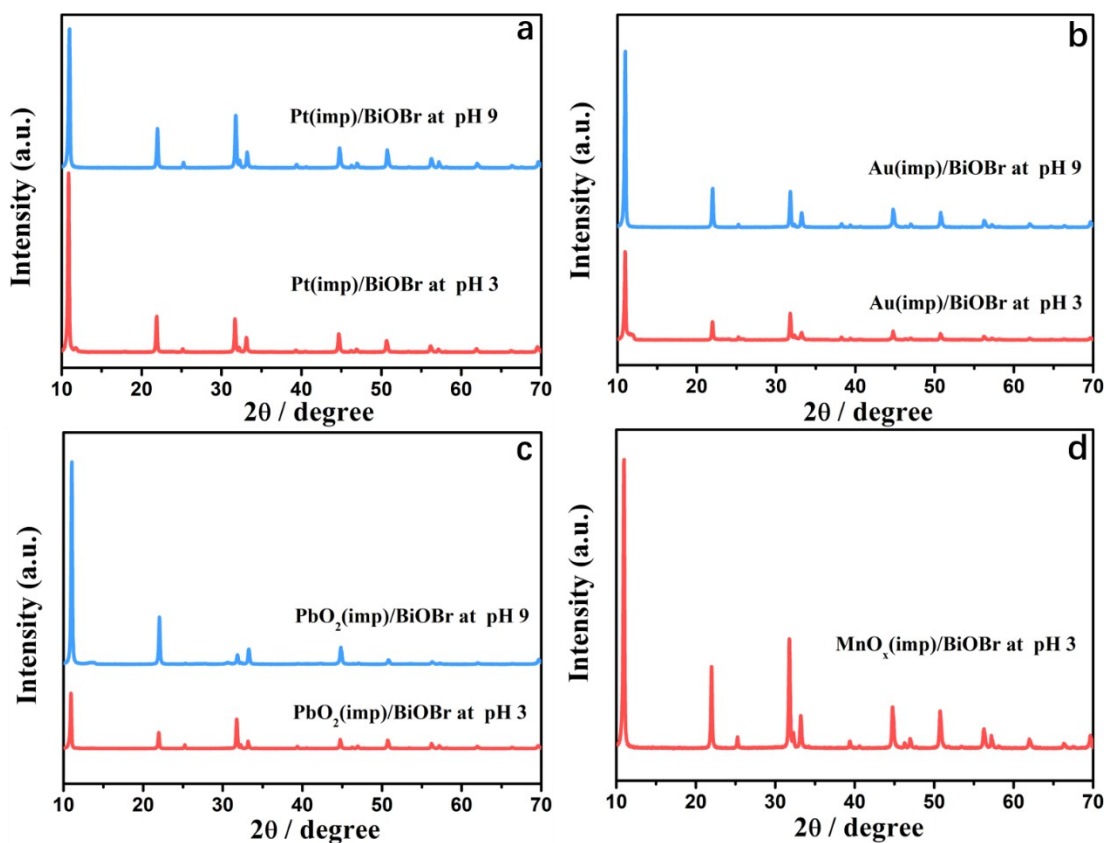


Figure S7. XRD patterns of typical samples obtained by impregnation at different pH values.

Characterization by X-ray photoelectron spectroscopy

XP spectra of Pt-modified BiOBr are shown in Figure S8a. Obviously, the characteristic Pt 4f line changes from a mixture of Pt in its metallic state (Pt^0) and oxidized Pt(Pt^{x+}) state at low pH values, to entirely oxidized Pt for depositions performed at elevated pH. Likewise, at low pH values Au is exclusively present in its metallic state as indicated by the Au 4f_{7/2} at BE = 84 eV (Figure S8c). Already at moderate pH (pH 7) a shift towards higher binding energies is observed and at high pH (pH 9) the characteristic Au 4f_{7/2} signal consists of two clearly distinguishable signals. These observations clearly indicate that Pt and Au nanoparticles are obtained by photo-reduction at low pH, while the complete reduction of the Pt precursor appears to be more difficult. Similar

differences in oxidation states between Pt and Au were also observed by Li et al. and might be due to a relatively high degree of hydroxylation of the Pt and Au precursors¹.

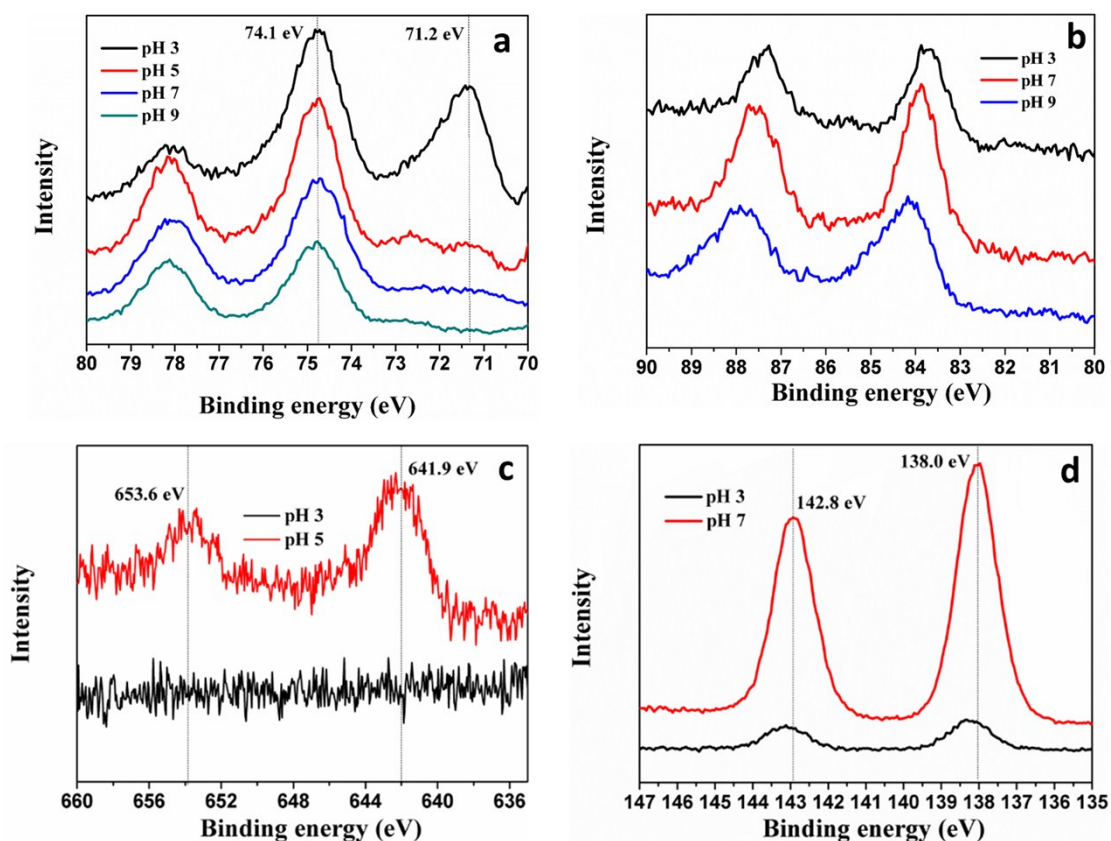


Figure S8. XPS spectra of BiOBr nanoparticles obtained after photodeposition at different pH (as indicated in the figure) of a) Pt nanoparticles, b) of Au nanoparticles, c) MnO_x, and d) PbO₂.

Theoretical Calculations

The electronic band structure of BiOBr was determined by density functional theory (DFT) calculations applying the Vienna Ab initio Simulation Package (VASP). The generalized gradient approximation of Perdew-Burke-Ernzerhof (GGA-PBE)² with van

der Waals correction proposed by Grimme (DFT-D2) was chosen due to its good description of long-range vdWals interactions. The energy cutoff is set to be 500 eV. All geometry structures were fully relaxed until the convergence criteria of energy and force were less than 10^{-5} eV and 0.04 eV/Å, respectively. The Monkhorst-Pack k-mesh of $9 \times 9 \times 9$ was adopted to represent the first Brillouin zone.

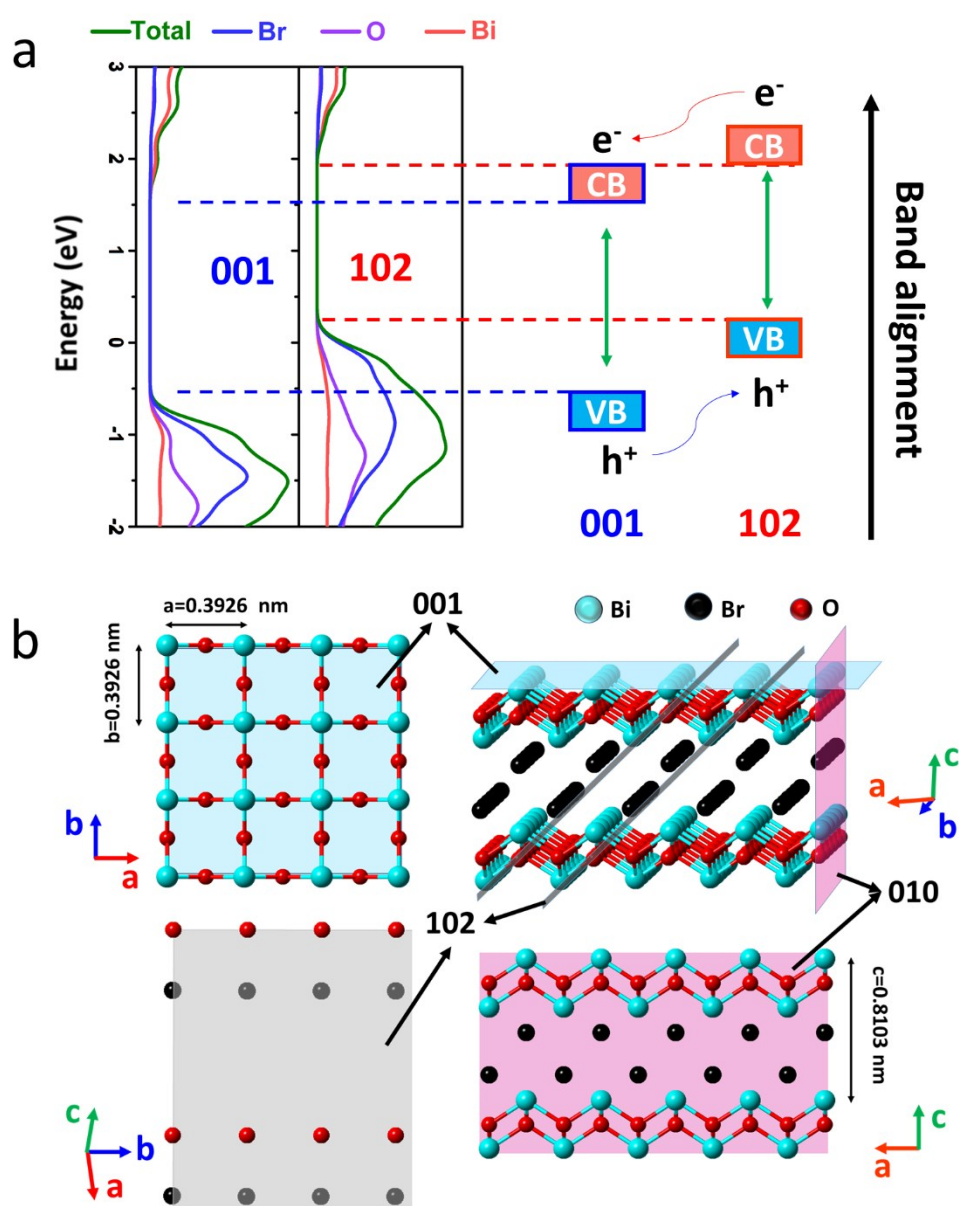


Figure S9. (a) Calculated density of states (DOS) and band alignment of the {001}, and {102}

facets of BiOBr. (b) Structural model illustration of BiOBr crystals, showing the three-dimensional projection, (001) facets, (010) facets and (102) facets.

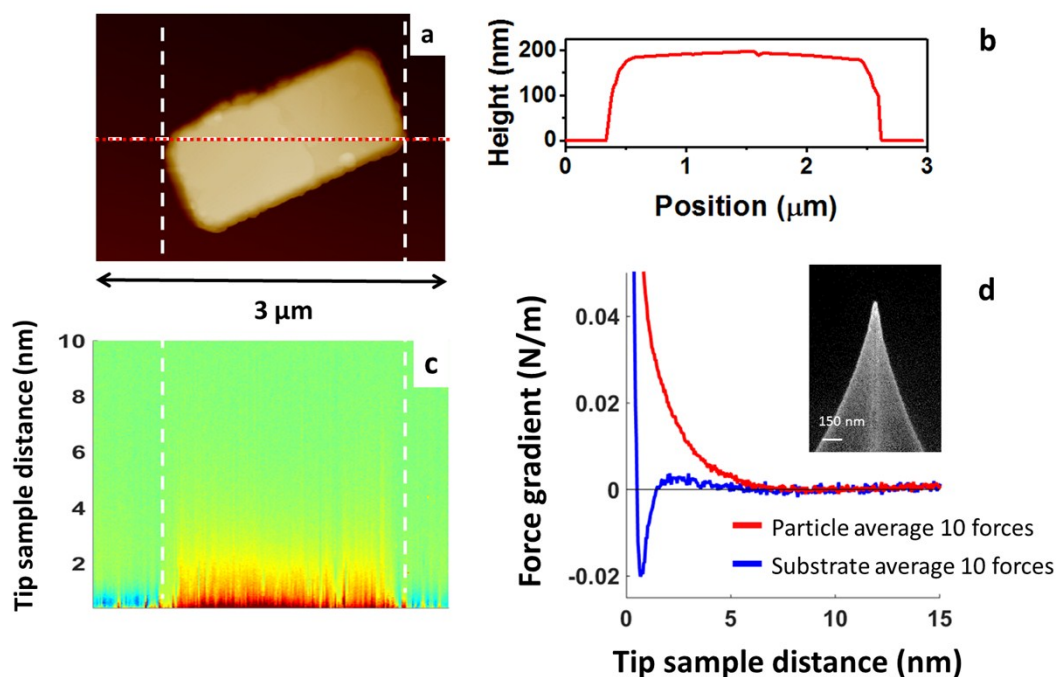


Figure S10. a) AM-AFM topography image of BiOBr particle adsorbed on Pt in a 10 mM NaCl solution at pH 6. b) Height profile taken along the red line in a). c) A 2D force versus distance plot of a BiOBr particle on Pt substrate in a 10 mM NaCl at pH 6 solution obtained by measuring 300 approaches. The color indicates the nature of the silica tip–sample interaction. Red indicates a repulsive interaction, whereas blue indicates an attractive interaction. On the BiOBr basal plane, the force monotonically increases from zero (green) to repulsive values (red) at a distance of several nanometers, as expected for two negatively charged surfaces immersed in 10 mM of NaCl solution at a $\text{pH} \approx 6$. Over the Pt substrate the force between tip and sample initially is weakly repulsive which suggest that Pt is weakly negatively charged; and at distance < 2 nm the tip experience an attractive force (blue) due Van der Waals forces. d) 2D plot of selected approaches located on the BiOBr basal plane (red) and Pt (blue) converted to force vs. distance curves. Scanning electron microscope image of the cantilever after being used in the experiment. The tip radius is estimated to be around 18 nm.

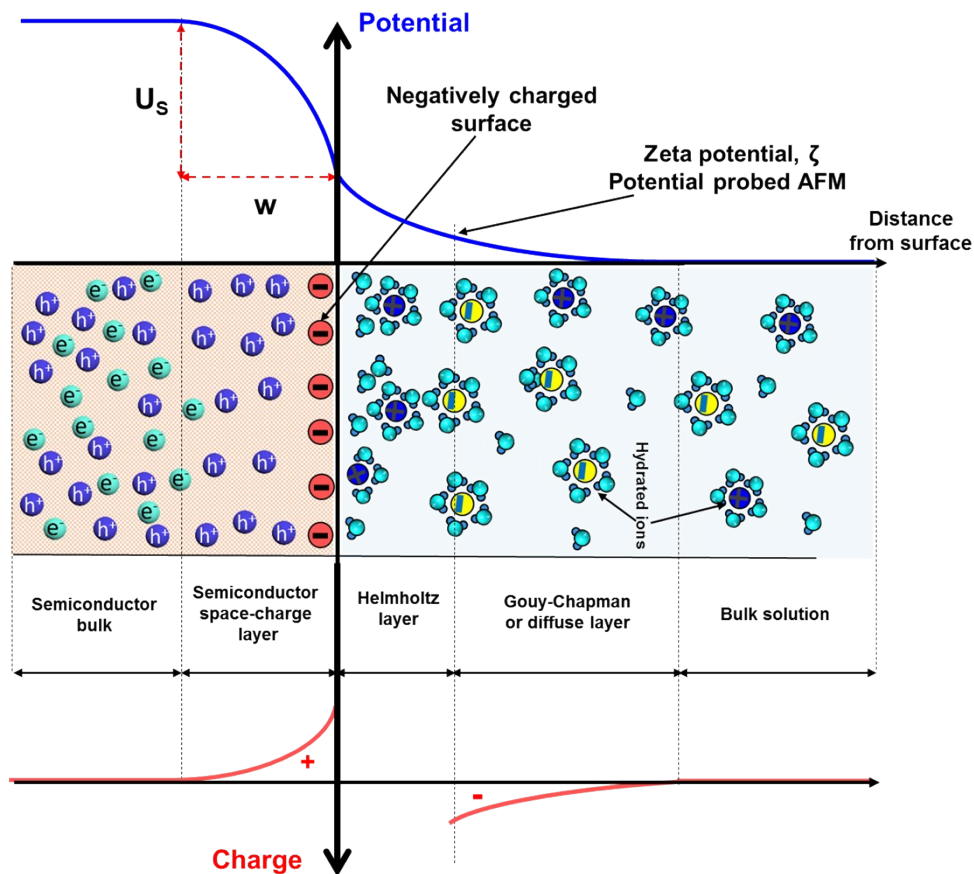


Figure S11. Schematic view of the electric double layers at the semiconductor/aqueous electrolyte interface with corresponding potential/charge distributions. U_s is the potential drop across the space-charge layer of width w .

References

- 1 Li, R. *et al.* Spatial separation of photogenerated electrons and holes among {010} and {110} crystal facets of BiVO₄. *Nature communications* **4**, 1432 (2013).
- 2 Perdew, J. P., Ernzerhof, M. & Burke, K. Generalized Gradient Approximation Made Simple. *Phys. Rev. Lett.* **77**, 3865, doi:10.1103/PhysRevLett.77.3865 (1996).